J. Plasma Phys. (2025), *vol*. 91, E81
 doi:10.1017/S0022377825000467

Ion cyclotron resonance frequency slow wave simulations in the Joint European Torus tokamak

D.L. Grekov

Institute of Plasma Physics, National Science Center, Kharkiv Institute of Physics and Technology, Kharkiv 61108, Ukraine

Corresponding author: D.L. Grekov, grekov@ipp.kharkov.ua

(Received 15 November 2024; revision received 13 April 2025; accepted 14 April 2025)

The propagation and absorption of the slow waves in the plasma of the Joint European Torus (JET) tokamak have been investigated by ray tracing. The study aims to obtain a qualitative notion of the penetration into the plasma and absorption of the slow wave excited by the A2 ITER-like antenna. The slow waves are radiated by antennas in the ion cyclotron resonance frequency inverted minority heating or mode conversion heating regimes. It has been discovered that the rays propagate in the toroidal direction over a significant distance, up to 6×10^3 cm, from the antenna. Spreading in the peripheral plasma, mainly between the separatrix and the wall, they slowly shift in the poloidal direction and can reach the divertor region. The change in equilibrium of the JET tokamak has a strong influence on both the propagation and absorption of slow waves. Absorption of the slow waves is caused by ion–electron collisions and Landau damping. In the minority heating regimes, the slow waves are strongly damped in the cyclotron resonance of minority ions even at very low minority density.

Key words: plasma heating, plasma simulation, plasma waves

1. Introduction

The main sources of plasma heating in the Joint European Torus (JET) are two systems: the neutral beam injection and radio frequency (RF) heating, the power of which is up to 15 MW (Rebut, Bickerton & Keen 1985 and many others). A system of antennas similar to the system that will be installed in the ITER has been developed to deliver RF power to the JET plasma (see Kaye *et al*. 1994). These antennas radiate two types of waves. One wave has an electric field vector perpendicular to the confining magnetic field. This is the so-called fast wave (FW). Hundreds of articles are devoted to the results of studies of plasma heating by this wave. The electric field vector of the other wave is parallel to the confining magnetic field. This is the slow wave (SW). Although the JET antennas are designed to prevent the excitation of this wave and are equipped with Faraday shields, it accounts

for approximately 10 % of the radiated power (Sato, Sawaya & Adachi 1988). A detailed analysis of the excitation of a SW by a shielded ITER-like antenna is given in the paper by Lyssoivan *et al*. (2012). Being expanded in the Fourier series in poloidal and toroidal angles, the parallel electric field can be divided into two parts. One part of the RF field forms the near field of the antenna (e.g. Myra 2021). The other part of the Fourier spectrum is radiated as the small-scale SW. What are the main characteristics of the SW in tokamak plasma? To answer this question, propagation and absorption of the SW were investigated, accounting for the real geometry of the JET tokamak. Modeling of propagation and absorption of the SW in areal tokamak has not been carried out before. It is impossible to solve this problem analytically or using simple one-dimensional models due to the complicated structure of the JET magnetic surfaces and confining field. Moreover, the numerical modeling of the full wave problem faces significant difficulties caused by the plasma inhomogeneity and problem stiffness. For example, a finite-difference time-domain modeling of Alcator C-Mod's field-aligned ICRF antenna takes 4–6 million processor core hours per run (Jenkins & Smithe 2015). On the other hand, for the typical JET plasma periphery parameters (electron density $n_e \sim 10^{11}$ cm^{-3} – 10^{12} cm^{-3} and electron temperature $T_e \sim$ 10–25 eV (Giroud *et al*. 2023)), the SW wavelength is much smaller than the average plasma radius. Therefore, the geometrical optics approximation can be applied to this analysis.

This paper is structured as follows. In § 2, the ray-tracing code SLOWAR-T is introduced and the initial conditions for the rays are analyzed. Section 3 first illustrates the intrinsic features of the SW propagation and absorption in the JET tokamak hydrogen plasma using as an example the rays that were launched in front of the center of the antenna. Next, the results of the investigation of the ray characteristics in the multi-species plasma are presented in § 4. Finally, the conclusions are drawn.

2. The SLOWAR-T simulations

2.1. *Equilibrium*

The scale of inhomogeneity of the plasma parameters in JET is much greater than SW wavelength. Therefore, the ray-tracing method (or approach) can be used for such simulations. Since during propagation, the SW 'feels' the plasma density and magnetic field locally, the equilibrium code EFIT (Lao *et al*. 1985) was used in order to reconstruct a JET equilibrium with one-zero divertor. The flux surface label is $\psi = 1$ at the last closed magnetic surface (LCMS) and $\psi = 0$ at the magnetic axis (figure 1).

The realistic shape of the JET vacuum vessel was taken into account while constructing a mathematical model of the plasma density distribution in the peripheral plasma. Two distinguished magnetic configurations were used in these calculations. One of them will be referenced as 'fat' and the other as 'thin' (see figure 2).

The plasma density and temperature profiles were set as

$$n(\psi) = \begin{cases} n_0 \frac{\exp(\xi_n) - \exp(A_n \xi_n \psi)}{\exp(\xi_n) - 1}, & \psi \le 1 \\ n_b + (n_x - n_b) \exp\left[(1-\psi)/\delta\right], & \psi > 1 \end{cases},$$

$$T(\psi) = \begin{cases} T_0 \frac{\exp(\xi_T) - \exp(A_T \xi_T \psi)}{\exp(\xi_T) - 1}, & \psi \le 1 \\ T_b + (T_x - T_b) \exp\left[(1-\psi)/\delta\right], & \psi > 1 \end{cases}, \qquad (2.1)$$

where n_0, T_0 are density and temperature at the axis, n_b, T_b are density and temperature at the plasma boundary, A_n, A_T are smoothing coefficients, n_x, T_x are density

https://doi.org/10.1017/S0022377825000467 Published online by Cambridge University Press

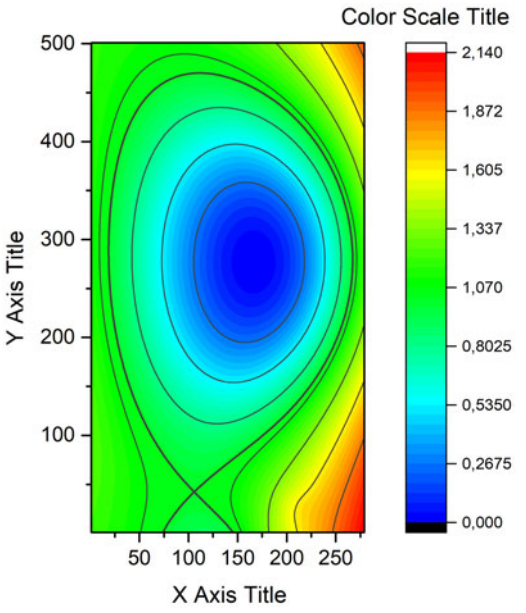

FIGURE 1. The magnetic surface label ψ distribution in the minor cross-section of the JET tokamak. 'Fat' equilibrium.

and temperature at the LCMS, ξ_n, ξ_T are variable parameters ($\xi_n = 4$ for density and $\xi_T = -2$ for temperature were chosen) and δ is the e-folding length outside the LCMS.

2.2. *Ray tracing*

Propagation and absorption of the SW in the JET plasma were studied using the ray-tracing code SLOWAR-T (SLOw WAve Rays in Tokamak). The SLOWAR-T code is the modified version of the code SLOWAR, described in Grekov (2024). The verification of the dispersion relation conservation shows that it fulfills the precision of the Runge–Kutta solver, which was used in the code. The code solves the equations

$$\frac{\mathrm{d}\vec{r}}{\mathrm{d}t} = \frac{\partial D_R}{\partial \vec{k}} \Big/ \frac{\partial D_R}{\partial \omega}, \quad \frac{\mathrm{d}\vec{k}}{\mathrm{d}t} = -\frac{\partial D_R}{\partial \vec{r}} \Big/ \frac{\partial D_R}{\partial \omega}, \tag{2.2}$$

where $\vec{k}$ is the wave vector, ω is the wave frequency, t is time, $\vec{r} = (X,\ Y,\ Z)$ are the Cartesian coordinates of the ray and $D(\omega, \vec{r}, \vec{k}) = 0$ is the dispersion equation

$$D = D_R + i D_I = \varepsilon_1 N_\perp^4 + \left[(\varepsilon_3 + \varepsilon_1)\left(N_{||}^2 - \varepsilon_1\right) + \varepsilon_2^2\right] N_\perp^2 + \varepsilon_3 \left[\left(N_{||}^2 - \varepsilon_1\right)^2 - \varepsilon_2^2\right] = 0. \tag{2.3}$$

Here, $k_{||} = \vec{k} \cdot \vec{B}/B$, $\vec{B}$ is the tokamak magnetic field, $N_{||} = ck_{||}/\omega$, $k_\perp = (k^2 - k_{||}^2)^{1/2}$ and $N_\perp = ck_\perp/\omega$. Cylindrical coordinates ($R,\ \phi,\ Z$) and quasi-toroidal coordinates ($r,\ \vartheta,\ \phi$) were also used in this investigation. Here, $R = \sqrt{X^2 + Y^2}$ is the

https://doi.org/10.1017/S0022377825000467 Published online by Cambridge University Press

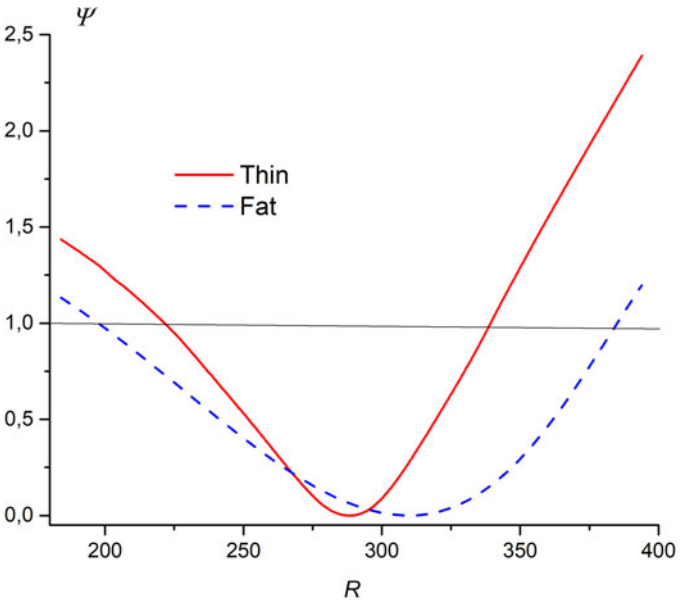

FIGURE 2. The magnetic flux label ψ as a function of big radius R along the line that passes through the magnetic axis.

big radius of the torus, $\phi = arctg(Y/X)$ is the toroidal angle, ϑ is the poloidal angle and r is the minor radius of the torus.

The calculation of the dielectric tensor $\hat{\varepsilon}$ is based on the warm plasma model and resolves only electron Landau damping and fundamental ion cyclotron resonance. For $(\omega - \omega_{c\alpha})^2)/(2k_{||}^2 v_{T\alpha}^2) >> 1$ the correction for the real part of ϵ_1 is negligible. For $((\omega - \omega_{c\alpha})^2)/(2k_{||}^2 v_{T\alpha}^2) \sim 1$, $\mathrm{Re}(\epsilon_1) \sim \mathrm{Im}(\epsilon_1)$, $D_I \sim D_R$ and the ray tracing is not applicable. The proper operator in the code terminates the calculation. Components of the tensor are defined as

$$\varepsilon_1 = 1 - \sum_\alpha \frac{\omega_{p\alpha}^2}{\omega^2 - \omega_{c\alpha}^2} + \sum_\alpha i\sqrt{\frac{\pi}{8}} \frac{\omega_{p\alpha}^2}{|k_{||}| v_{T\alpha} \omega} \exp\left[-\frac{(\omega - \omega_{c\alpha})^2}{2k_{||}^2 v_{T\alpha}^2}\right], \tag{2.4}$$

$$\varepsilon_2 = \sum_\alpha \frac{\omega}{\omega_{c\alpha}} \frac{\omega_{p\alpha}^2}{\omega^2 - \omega_{c\alpha}^2}, \tag{2.5}$$

$$\varepsilon_3 = 1 + \frac{\omega_{pe}^2}{k_{||}^2 v_{\mathrm{Te}}^2}\left[1 + i\sqrt{\pi} z_e W(z_e)\right] + i\varepsilon_{3\mathrm{coll}}, \tag{2.6}$$

where $\mathrm{m_b}$ and $\mathrm{e_b}$ are mass and charge of b particles, b=α, e $\omega_{p\alpha} = (4\pi e^2 n_\alpha / m_\alpha)^{1/2}$ is the plasma frequency of α ions, $\omega_{c\alpha} = eB/cm_\alpha$ is the α ion cyclotron frequency, $v_{T\alpha} = \sqrt{T_\alpha / m_\alpha}$ is the α ion thermal velocity, $\omega_{pe} = (4\pi e^2 n_e / m_e)^{1/2}$ is the plasma frequency of electrons, $v_{\mathrm{Te}} = \sqrt{T_e / m_e}$ is the thermal velocity of electrons, $z_e = \omega/\sqrt{2}|k_{||}|v_{\mathrm{Te}}$, $W(z_e)$ is the plasma dispersion function, $\varepsilon_{3\mathrm{coll}} = \omega_{pe}^2 \nu_{\mathrm{eff}}/\omega^3$, ν_{eff} is the effective collisional frequency of electrons where $\nu_{eff} = (4/3)\sqrt{2\pi/m_e}(e^4 Z^2 \wedge n_e)/(T_e^{3/2})$ and Λ is the Coulomb logarithm.

https://doi.org/10.1017/S0022377825000467 Published online by Cambridge University Press

Seeing $|\varepsilon_3| >> |\varepsilon_1|,\ |\varepsilon_2|$, the solutions of equation (2.3) are

$$N_{\perp S}^2 = -\varepsilon_3 \left(N_{||}^2 - \varepsilon_1\right)/\varepsilon_1, \tag{2.7}$$

for the SW and

$$N_{\perp F}^2 = \left[\left(N_{||}^2 - \varepsilon_1\right)^2 - \varepsilon_2^2\right] / \left(\varepsilon_1 - N_{||}^2\right), \tag{2.8}$$

for the FW. Equations (2.7) and (2.8) are correct outside the conversion region, where $\varepsilon_1 \approx N_{||}^2$. Strictly speaking, ray tracing is not applicable in the regions of ray reflection and mode conversion regions. In the region of reflection of the SW from Maxwell's equations for the $E_{||}$ field of the SW the equation $(\mathrm{d}^2 E_{||}/\mathrm{d}\xi^2) + \left(\mathrm{d}k_{\perp S}^2/\mathrm{d}\xi\right)_{\xi ref} (\xi - \xi_{\mathrm{ref}})\, E_{||} = 0$ is valid. Here, ξ is the coordinate in the direction of the gradient of $(N_{||}^2 - \varepsilon_1)$. This equation is transformed to the Airy equation $(\mathrm{d}^2 E_{||}/\mathrm{d}\varsigma^2) + \varsigma E_{||} = 0$, where $\varsigma = (\xi - \xi_{\mathrm{ref}}) \left((\mathrm{d}k_{\perp S}^2/\mathrm{d}\xi)\right)_{\xi \mathrm{ref}}^{\frac{1}{3}}$. It follows that the reflection occurs in the region $\varsigma \sim 1$, or $\left|\xi - \xi_{ref}\right| \approx \Delta r \sim \left((\mathrm{d}k_{\perp S}^2/\mathrm{d}\xi)\right)_{\xi ref}^{-\frac{1}{3}}$. For the selected modeling parameters, $\Delta r \sim 1\mathrm{cm}$. Beyond this region, the Airy function connects to the ray-tracing solutions. Thus, using the ray-tracing model only leads to inaccuracy in determining the phase only, which is of the order of π. Such a value of imprecision is insignificant for the present consideration. As $\varepsilon_3 < 0$ at $n_e \geq 10^7 \mathrm{cm}^{-3}$, the SW propagates in peripheral plasma only if the conditions $0 < \varepsilon_1 < N_{||}^2$ are fulfilled. Both of these inequalities are satisfied in hydrogen plasmas with ion cyclotron resonance frequency (ICRF) inverted minority heating (MH) or mode conversion heating (MC) regimes (Start *et al*. 1999; Lamalle *et al*. 2006; Mayoral *et al*. 2006). A key feature of these so-called inverted scenarios is that the minority ion species have a smaller charge-to-mass ratio than the majority ion species, i.e. $Z_{\mathrm{min}}/A_{\mathrm{min}} < Z_{\mathrm{maj}}/A_{\mathrm{maj}}$. The wave frequency and the toroidal magnetic field are chosen so that the cyclotron resonance of the majority ions is located outside the plasma on the outer side of the torus in these experiments.

The power associated with a certain ray Q is defined as $Q = Q_0 e^{-}$, where Q_0 is the initial RF power at the ray start location and $\Gamma = \int_0^t \gamma\, \mathrm{d}t$, $\gamma = -(D_I)/(\partial D_R/\partial\omega)$. When calculating Q along the ray, electron Landau damping p_e, ion cyclotron damping $p_{i\alpha}$ ($\alpha = 1, 2, 3$) and collisional damping p_{col} were taken into account. The power dissipated along the ray P_{tot} was defined as $P_{tot} = Q_0(1 - e^{-})$. It can be represented as $P_{tot} = \int_0^s (p_{\mathrm{col}} + p_e + p_{i1} + p_{i2} + p_{i3})ds$, where $s = \int_0^t |\vec{v}_g|\mathrm{d}t$ is the ray length. In what follows we assume $Q_0 = 1$.

2.3. *Initial conditions*

To define $\vec{k}_0$ for SW ray tracing, the distribution of the wave electric field E_φ at the ICRF antenna must expanded into a Fourier series of poloidal (wavenumber m_0) and toroidal (wavenumber l_0) angles. It allows us to determine $N_{\phi 0}$ as $N_{\phi 0} = (cl_0)/(\omega R_0)$. The value of N_{z0} was defined as $N_{z0} = (cm_0/\omega\overline{a})\cos\left[arctg\,(Z_0/R_0)\right]$, where $|m_0| \leq 50$, $|Z_0| \leq 50cm$, and $\overline{a} \approx 100cm$ is a mean minor radius. Accounting for $N^2 = N_R^2 + N_\phi^2 + N_z^2$ and

$$N_{||} = N_R b_R + N_\phi b_\phi + N_z b_z, \tag{2.9}$$

where (b_R, b_ϕ, b_z) are the components of the unit vector, which is parallel to the tokamak magnetic field, the initial value N_{R0} was determined from the dispersion

https://doi.org/10.1017/S0022377825000467 Published online by Cambridge University Press

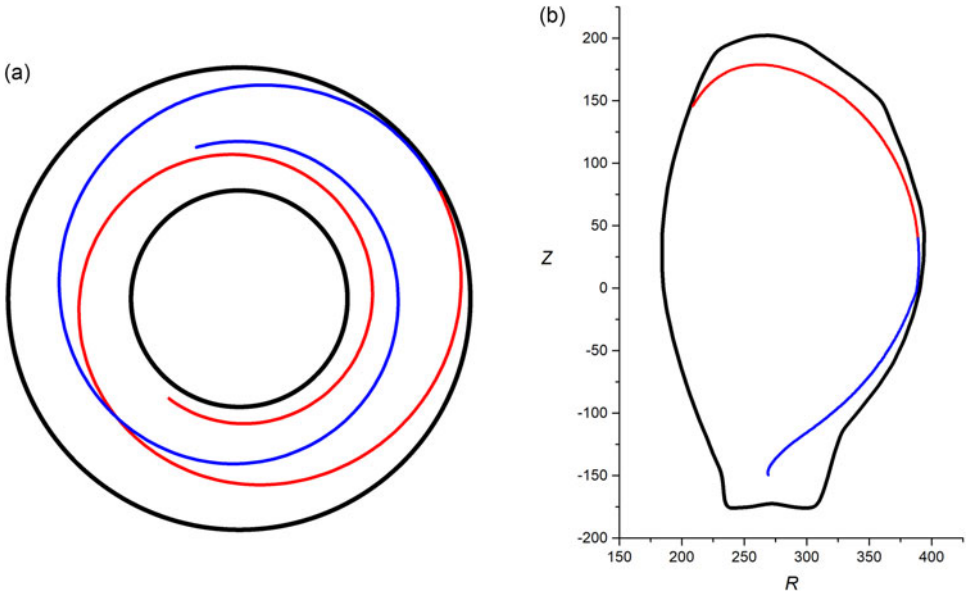

FIGURE 3. The SW rays in the equatorial (a) and minor (b) cross-sections of the torus for $l_0 = -40$, $m_0 = 2$, second root – red lines and for $l_0 = +40$, $m_0 = 2$, first root – blue lines. 'Fat' equilibrium.

equation (2.3). Four roots of (2.3) were found by iterations, taking Re$[W(z_e)]$ in ε_3 and assuming $N_{R0} = 0$ in $k_{||}$ at the first step. At subsequent iterations, the value N_{R0} from the previous iteration was substituted into ε_3. Two of the roots correspond to the FW. They are complex for the chosen value of ψ_0. The other two roots are real in the inverted scenarios and correspond to the SW . Let us call the smaller one the first root and the larger one the second root.

3. Features of the SW propagation and absorption in the JET tokamak

3.1. *Intrinsic features of the SW. Pure hydrogen plasma*

The following set of parameters has been used for consideration in this subsection: $B_0 = 39$ kG, $n_{e0} = 1 \times 10^{13}$ cm^{-3}, $n_x = 4 \times 10^{11}$ cm^{-3}, $n_{eb} = 1 \times 10^{11}$ cm^{-3}, $n_H/n_e = 1.0$, $T_{e0} = 3$ keV, $T_x = 60$ eV, $T_{eb} = 10$ eV, $f = \omega/2\pi = 32$ MHz, the 'fat' equilibrium. The ray starts from a fixed point $R_0 = 389$ cm, $Z_0 = 40$ cm which in Z direction is very close to the magnetic axis.

As can be seen from figure 3(a), the SW propagates predominantly in the toroidal direction. The JET tokamak antenna system consists of two systems spaced at a toroidal angle of π (Kaye *et al*. 1994). Therefore, the RF power emitted as SWs is uniformly distributed in the toroidal direction. In this case, the angular displacement in the poloidal direction is relatively small, of the order of π /4 (see figure 3b). This is the essential difference between SWs in the ion cyclotron frequency range and lower hybrid SWs. The latter, when propagating in tokamaks, perform many reversals in the poloidal direction (Baranov & Fedorov 1980). Also, figure 3(b) shows that SWs propagate along the periphery of the plasma and can penetrate into the divertor region.

https://doi.org/10.1017/S0022377825000467 Published online by Cambridge University Press

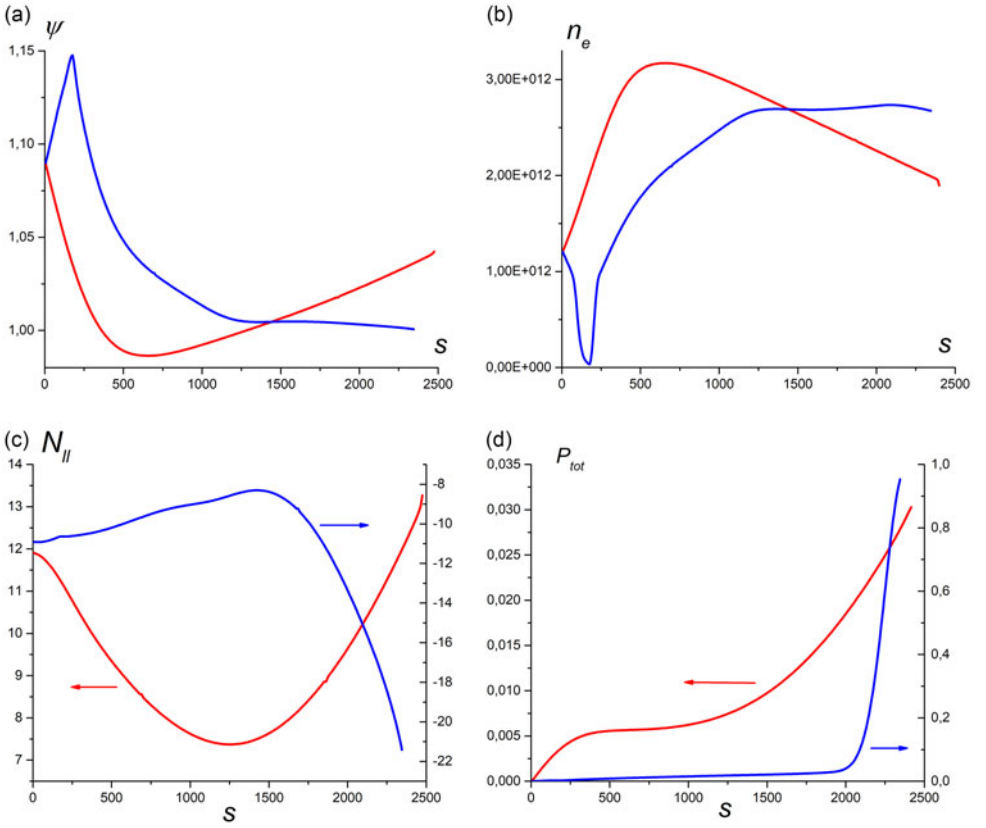

FIGURE 4. The flux label (*a*), the plasma density (*b*), the refractive index parallel to the magnetic field (*c*) and the total absorbed power (*d*) *vs.* the ray length for $l_0 = -40$ – red lines and for $l_0 = +40$ – blue lines. 'Fat' equilibrium.

The SWs moving in the $co - \vec{B}$ direction ($N_{||} > 0$, red lines in figures 3 and 4) propagate in the direction of increasing plasma density (figures 4*a* and 4*b*). The SWs have anomalous dispersion. The group velocity $v_{g\nabla\psi} < 0$ together with $N_{\nabla\psi} > 0$ at the initial part of the ray $s < 550$ cm. The maximum density at which $\varepsilon_1 = N_{||}^2$ or $N_{\nabla\psi} = 0$ is more than 3×10^{12} cm^{-3}. Since for these waves the maximum value of $N_{||}$ is less than 14, their Landau damping is negligible. The collisional damping (figure 4*d*) is also rather small.

The SWs moving in the *counter* $- \vec{B}$ direction ($N_{||} < 0$, blue lines in figures 3 and 4) propagate in the direction of the wall at first. After reflection from the wall, they slowly penetrate towards higher-density plasma. The maximum achieved density of 2.5×10^{12} cm^{-3} is comparable to the former case. The absolute value of $N_{||}$ is strongly increasing at the final section of the ray. This leads to complete absorption of the SW due to Landau damping in the divertor region.

3.2. *Influence of plasma density changes*

In this subsection, we will study how the variation of the plasma density profile affects the propagation of the SWs. For this purpose, all parameters were fixed as

https://doi.org/10.1017/S0022377825000467 Published online by Cambridge University Press

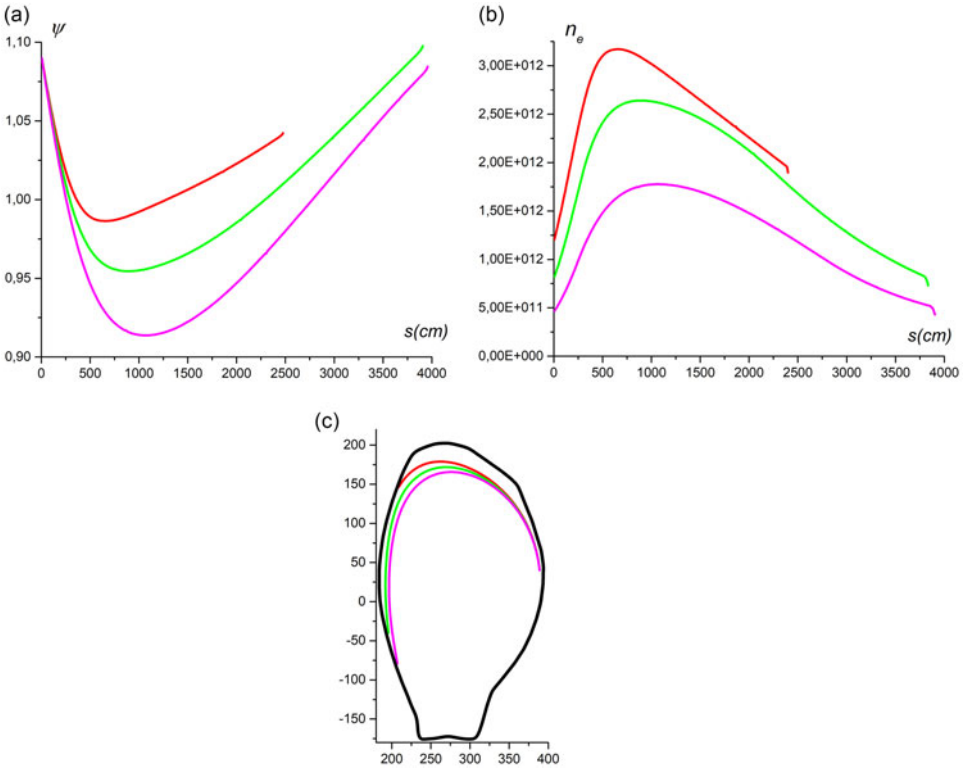

FIGURE 5. The flux label (*a*) and the plasma density (*b*) *vs.* the ray length for $\xi_n = 4$ (red), $\xi_n = 2$ (green) and $\xi_n = 0$ (magenta), $l_0 = -40$. 'Fat' equilibrium. The SW rays in the minor cross-section (*c*) for the same set of parameters.

in the previous subsection. At first, the parameter ξ_n in equation (2.1) was reduced from 4 to 0. In this case, the density profile changes from very flat to parabolic.

As can be seen from figure 5(*a*), as ξ_n decreases, the minimum value of ψ decreases, too. This means that the SW penetrates closer and closer to the magnetic axis. However, the maximum value of the plasma density on the ray, which increases with decreasing ψ, still declines (figure 5*b*). The path in the poloidal section of the torus, taken by the SW along the periphery of the plasma, increases significantly (figure 5*c*). The number of revolutions of the SW around the torus also increases.

Now the influence of the plasma density value on the magnetic axis on the wave propagation will be studied. The parameter ξ_n is equal to 4, as before. As can be seen from figures 6(*a*) and 6(*b*), a trend similar to figure 5 is observed again. The decrease in plasma density in the center also leads to an increase in the penetration depth of the wave. And the maximum density value achievable by the SW also decreases.

3.3. *Effect of the initial poloidal wavenumber m_0*

As can be seen from figure 16 of the paper by Kaye *et al*. (1994), the JET tokamak antenna is shielded by a screen consisting of 46 conductors. The complex structure of the electric field penetrating through such a screen can be seen in

https://doi.org/10.1017/S0022377825000467 Published online by Cambridge University Press

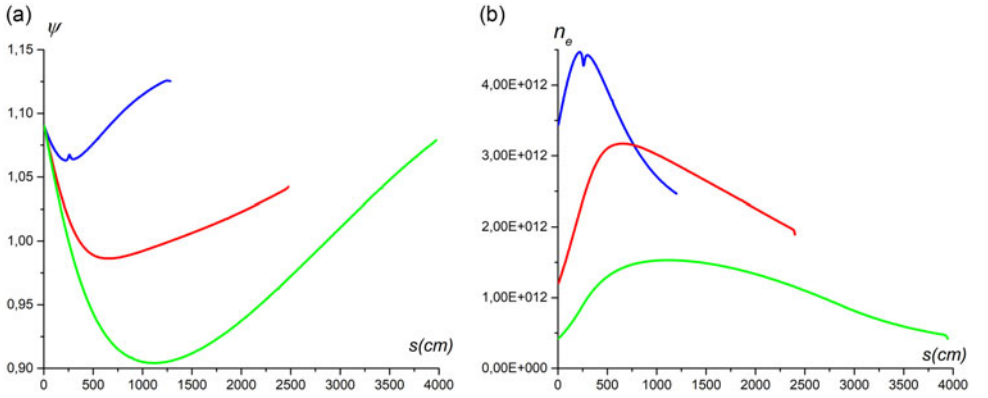

FIGURE 6. The flux label (*a*) and the plasma density (*b*) *vs.* the ray length for $n_{e0} = 3 \times 10^{13}$ cm^{-3} (blue), $n_{e0} = 1 \times 10^{13}$ cm^{-3} (red) and $n_{e0} = 3 \times 10^{12}$ cm^{-3} (green), $l_0 = -40$. 'Fat' equilibrium.

figure 2 of Lyssoivan *et al*. (2012). When such a field is expanded in a series by poloidal wavenumbers, harmonics with an initial $|m_0|$ of the order of 40 appear. The influence of such m_0 is shown in figure 7 for $l_0 = +40$.

As shown in figure 7(*a*), the initial m_0 has a strong effect on the initial $N_{||}$. At $m_0 = 50$, the initial $N_{||}$ becomes even larger than shown in the figure. At $m_0 = -50$, the SW is not emitted because the initial $N_{||}$ is too small. As can be seen from figure 7(*b*), the collisional damping of the SW is small, of the order of several percent, in all cases. The increase in absorption for the case of $m_0 = 30$ is associated with the large values of $N_{||}$ at the initial section of the trajectory. This leads to Landau damping of the SW on electrons. As follows from figure 7(*c*), the larger the initial value of m_0, the longer the path along the plasma periphery the SW travels before hitting the wall.

3.4. *The SW in the 'fat' and 'thin' magnetic configurations*

As can be seen from figure 2, in the 'thin' magnetic configuration, the region of low-density plasma between the separatrix and the wall, where the propagation of a SW is possible, is much wider than in the 'fat' configuration. The length of the ray in the 'thin' case is more than twice the length of the ray in the 'fat' case (figure 8*a*). The first turn of the SW around the torus passes through low-density plasma. Then the plasma density along the ray path increases and reaches one third of the density on the magnetic axis (figure 8*b*).

Increasing $|N_{||}|$ along the ray path (figure 8*c*) leads to rapid absorption of the SW due to Landau damping in both cases. In the 'thin' case, this is preceded by the absorption of a small, approximately 20 %, part of the RF power due to collisional damping (figure 8*d*). In contrast to the 'fat' case, in the 'thin' case the propagation and absorption of the SW weakly depends on the initial value of m_0.

4. The slow wave in the multi-species plasma

The § 3 set of parameters is used in this section except for $B_0 = 34.5$ kG, 'thin' equilibrium. Hydrogen (H) plasmas with minority species such as deuterium (D)

https://doi.org/10.1017/S0022377825000467 Published online by Cambridge University Press

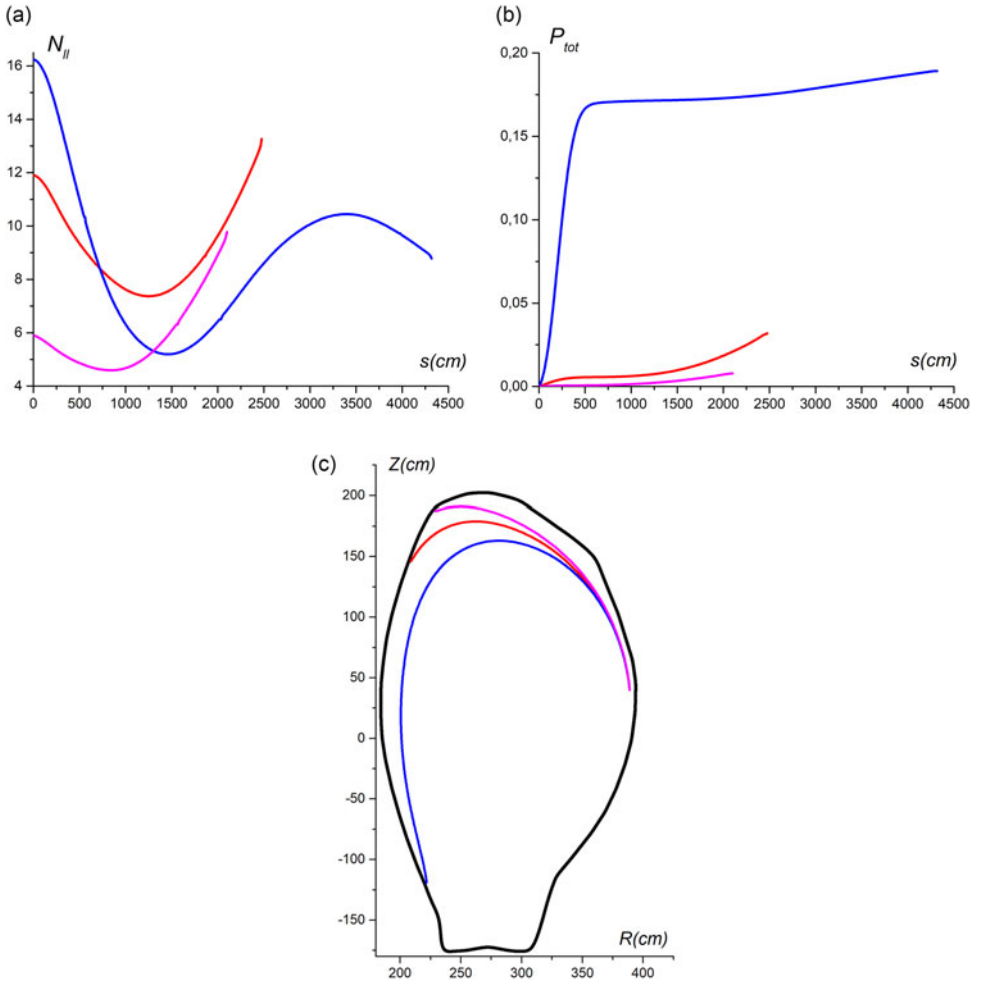

FIGURE 7. The refractive index parallel to the magnetic field (*a*) and the total absorbed power (*b*) *vs.* the ray length for $m_0 = 2$ – red, $m_0 = -30$ – blue and $m_0 = +30$ – magenta. The SW rays in the minor cross-section (*c*) for the same set of parameters. 'Fat' equilibrium, $l_0 = -40$.

and/or helium (3He) are under investigation. With this choice of parameters, the cyclotron resonance of H is located outside the plasma on the outer side of the torus. The cyclotron resonance of 3He is located at R_{3He}= 317 cm, and the cyclotron resonance of D is at $R_D = 238$ cm.

The D minority affects neither the SW propagation (cf. figure 8*a* and figure 9*a*) nor the SW absorption (cf figure 8*d* and figure 9*b*).

Just as in H plasma, the SW is absorbed due to collisions and Landau damping before it reaches the D–H hybrid resonance.

The 3He minority as a third ion species completely changes the SW pattern. At very low densities $n_{3He}/n_e < k_{||}\rho_{L3He}$, the cyclotron absorption of the wave by 3He ions increases with increasing n_{3He}/n_e and at $n_{3He}/n_e \approx 0.25\,\%$ reaches 100 % (figure 10*a*). Here, ρ_{L3He} is the Larmor radius of the ^{3}He ions.

These calculations are confirmed by the following estimates. The width of the cyclotron resonance ΔR_c is approximately equal to $\Delta R_c \approx C k_{||}\rho_{L3He} R$, where C is

https://doi.org/10.1017/S0022377825000467 Published online by Cambridge University Press

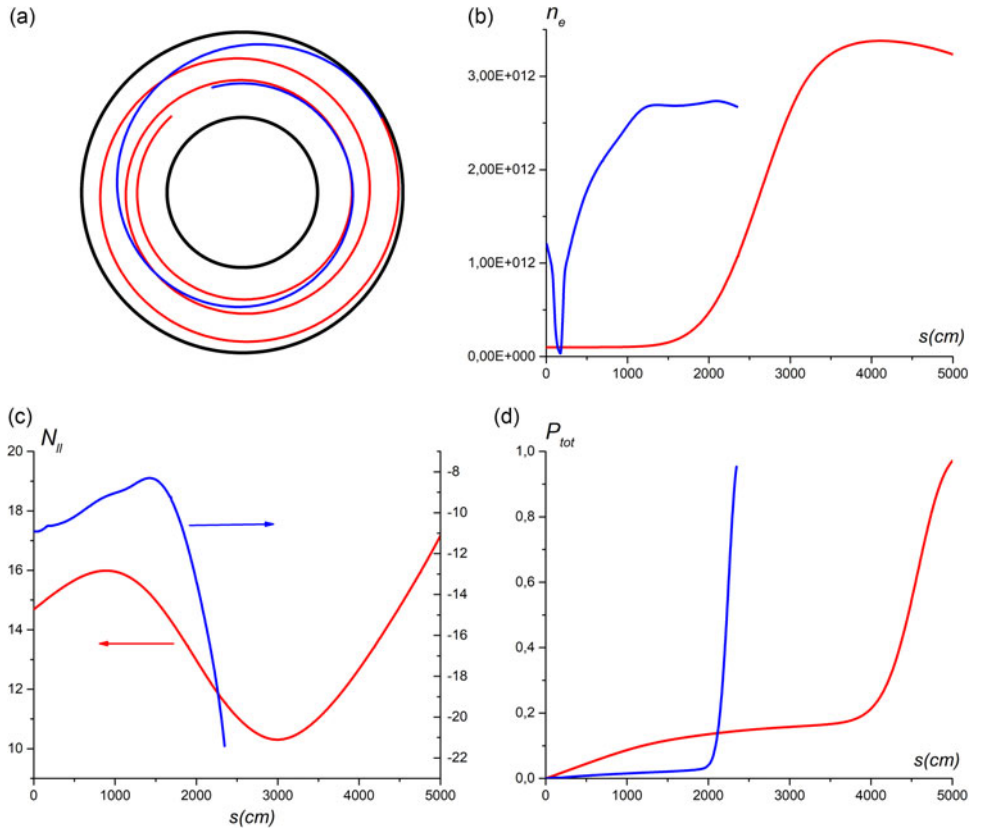

FIGURE 8. The SW rays in the equatorial cross-section (*a*), the plasma density (*b*), the refractive index parallel to the magnetic field (*c*) and the total absorbed power (*d*) *vs.* the ray length. 'Thin' equilibrium – red, 'Fat' equilibrium – blue.

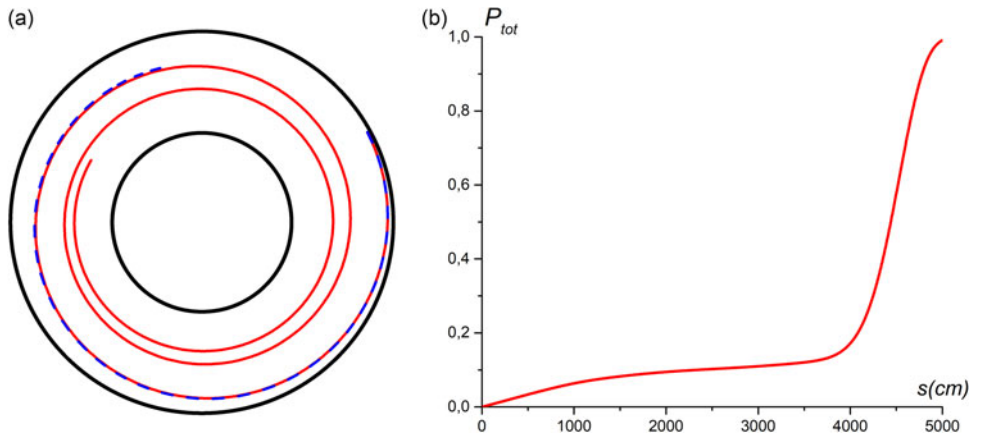

FIGURE 9. The SW rays in the equatorial cross-section (*a*); the total absorbed power *vs.* the ray length (*b*). 'Thin' equilibrium. Shown are D (4 %) + H (96 %) plasma – red; D (4 %) + 3He (1 %) + H (94 %) plasma – blue, dashed.

https://doi.org/10.1017/S0022377825000467 Published online by Cambridge University Press

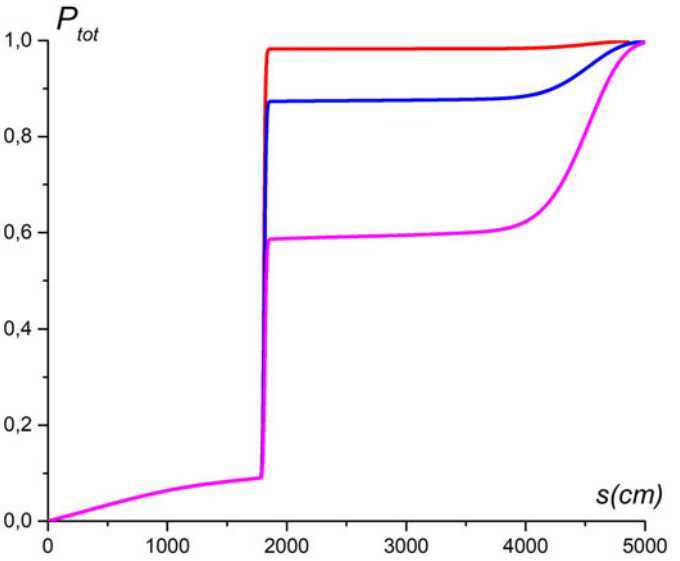

FIGURE 10. The total absorbed power *vs.* the ray length. 'Thin' equilibrium. Shown are D (4 %) + 3He + H plasma; 3He (0.05 %) – magenta, 3He (0.125 %) – blue; and 3He (0.25 %) – red.

a constant of the order of 1. The time Δt_c it takes for the ray to pass through the cyclotron resonance is estimated as $\Delta t_c \approx \Delta R_c / v_{g\nabla\psi}$, where $v_{g\nabla\psi} \sim v_{g||}\sqrt{m_e/M_i}$ (Grekov *et al.* 2024) and $v_{g||} \sim c/N_{||}$. The optical thickness τ using these estimates is $\tau = \gamma \Delta t_c = \frac{\mathrm{Im}\varepsilon_1}{\mathrm{Re}\varepsilon_1}\omega \Delta t_c \approx C n_{3He}/n_e \times \omega R / v_{g\nabla\psi}$. Setting $\tau = 1$, we obtain $n_{3He}/n_e \approx 0.2\,\%$, which agrees well with the calculations. With a further increase in 3He density, it makes a non-negligible contribution to the dispersion of the SW. Between cyclotron resonances H and 3He, an ion–ion hybrid resonance appears. In this region, the dispersion equation (3) is not applicable, and the calculations were stopped (figure 9*a*). To describe the SW in this case correctly, it is necessary to use the full kinetic dielectric tensor. Such consideration will be done elsewhere.

5. Conclusion

The features of the SWs' propagation and absorption in the plasma of the JET tokamak have been investigated by ray tracing. The SWs are radiated by antennas in ICRF inverted MH or MC regimes. The SW rays propagate mainly in the toroidal direction for a distance of up to 6×10^3 cm along and against the direction of the magnetic field. Spreading in the peripheral plasma, mainly between the LCMS and the wall, they slowly shift in the poloidal direction and can reach the divertor region. The change in equilibrium of the JET tokamak has a strong influence on both the propagation and absorption of the SWs. As the distance between the separatrix and the wall increases, the length of the rays increases. Collisional damping of the wave appears. The dependence of the propagation and absorption of the SW on the initial value of the poloidal wavenumber weakens. Cyclotron damping on H and D ions of these waves in the peripheral plasma is negligibly small. Absorption of the SWs is caused by ion–electron collisions and Landau damping. In the MH three-ion regimes, D-3He-H, the SWs are strongly damped in the cyclotron resonance of 3He ions. The cyclotron absorption of the wave by 3He ions increases with

https://doi.org/10.1017/S0022377825000467 Published online by Cambridge University Press

increasing n_{3He}/n_e and at $n_{3He}/n_e \approx 0.25\,\%$ reaches 100 %. With a further increase in 3He density, it makes a non-negligible contribution to the dispersion of the SW. To describe the SW in this case correctly, it is necessary to use the full kinetic dielectric tensor. Such consideration will be done elsewhere.

Acknowledgment

Y. Volkova is thanked for her assistance in preparing the manuscript.

Editor Peter Catto thanks the referees for their advice in evaluating this article.

Funding

This work was supported by 'Cambridge – NFDU 2022. Individual research (development) grants for Ukrainian scientists (supported by the University of Cambridge, Great Britain)' within the research project N 232/0022.

Declaration of interests

The authors report no conflict of interest.

REFERENCES

BARANOV, Y.F. & FEDOROV, V.I. 1980 Lower-hybrid wave propagation in tokamaks. *Nucl. Fusion* **20** (9), 1111–1118.

GIROUD, C. *et al.* 2023 Core-edge integrated neon-seeded scenario in deuterium-tritium at JET. IAEA-CN-316/EX-P/P5/2322.

GREKOV, D., ALBERT, C., TURKIN, YU. & VOLKOVA, YU. 2024 Modelling of ICRH slow wave propagation and absorption in wendelstein 7-x stellarator. *Nucl. Fusion* **64** (10), 106016.

JENKINS, T.G. & SMITHE, D.N. 2015 High-performance computational modeling of plasma-surface interactions and RF antennas. *AIP Conf. Proc* **1689**, 030003.

KAYE, A., BROWN, T., BHATNAGAR, V., CRAWLEY, P., JACQUINOT, J., LOBEL, R., PLANCOULINE, J., REBUT, P.-H., WADE, N. & WALKER, C. 1994 Present and future JET ICRF antennae. *Fusion Engng Des.* **24** (1-2), 1–21.

LAMALLE, P.U. *et al.* 2006 Expanding the operating space of ICRF on JET with a view to ITER. *Nucl. Fusion* **46** (2), 391–400.

LAO, L.L., JOHN, H.S., STAMBAUGH, R., KELLMAN, A. & PFEIFFER, W. 1985 Reconstruction of current profile parameters and plasma shapes in tokamaks. *Nucl. Fusion* **25** (11), 1611–1622.

LYSSOIVAN, A. *et al.* 2012 Simulation of ITER full-field ICWC scenario in JET: RF physics aspects. *Plasma Phys. Control. Fusion* **54** (7), 074014.

MAYORAL, M.-L. *et al.* 2006 Hydrogen plasmas with ICRF inverted minority and mode conversion heating regimes in the JET tokamak. *Nucl. Fusion* **46**, S550–S563.

MYRA, J.R. 2021 A tutorial on radio frequency sheath physics for magnetically confined fusion devices. *J. Plasma Phys.* **87** (5), 905870504.

REBUT, P.H., BICKERTON, R.J. & KEEN, B.E. 1985 The joint European torus: installation, first results and prospects. *Nucl. Fusion* **25** (9), 1011–1022.

SATO, Y., SAWAYA, K. & ADACHI, S. 1988 Faraday shield effects on a half-turn loop antenna used for ICRF plasma heating. *IEEE Trans. Plasma Sci.* **16** (5), 574–580.

START, D.F.H. *et al.* 1999 Bulk ion heating with ICRH in JET DT plasmas. *Nucl. Fusion* **39** (3), 321–336.